The Cryosphere Discuss., 9, 3137–3163, 2015
www.the-cryosphere-discuss.net/9/3137/2015/
doi:10.5194/tcd-9-3137-2015

The Cryosphere Discussions
Open Access

The importance of a surface organic layer in simulating permafrost thermal and carbon dynamics

E. Jafarov and K. Schaefer

National Snow and Ice Data Center, Cooperative Institute for Research in Environmental Sciences, University of Colorado at Boulder, Boulder, CO 80309, USA

Received: 4 May 2015 – Accepted: 19 May 2015 – Published: 12 June 2015

Correspondence to: E. Jafarov (elchin.jafarov@colorado.edu)

Published by Copernicus Publications on behalf of the European Geosciences Union.

Abstract

Permafrost-affected soils contain twice as much carbon as currently exists in the atmosphere. Studies show that warming of the perennially frozen ground could initiate significant release of the frozen soil carbon into the atmosphere. To reduce the uncertainty associated with the modeling of the permafrost carbon feedback it is important to start with the observed soil carbon distribution and to better address permafrost thermal and carbon dynamics. We used the recent Northern Circumpolar Soil Carbon Dataset to simulate present soil organic carbon (SOC) distribution in permafrost-affected soils under the steady state climate forcing. We implemented a dynamic surface organic layer with vertical carbon redistribution and dynamic root growth controlled by active layer thickness to improve modeling of the permafrost thermodynamics. Our results indicate that a dynamic surface organic layer improved permafrost thermal dynamics and simulated active layer thickness, allowing better simulation of the observed SOC densities and their spatial distribution.

1 Introduction

Warming of the global climate will lead to widespread permafrost thaw and degradation with impacts on ecosystems, infrastructure, and emissions to amplify climate warming (Oberman, 2008; Callaghan et al., 2011; Shuur et al., 2015). Permafrost affected soils contain 1700 Gt of carbon, where about 800 Gt of carbon is preserved, frozen in permafrost (Tarnocai et al., 2009; Hugelius et al., 2014). As permafrost thaws, organic matter frozen within permafrost will thaw and decay, which will initiate the permafrost carbon feedback (PCF), releasing an estimated 120 ± 85 Gt of carbon emissions by 2100 (Schaefer et al., 2014). The wide range of estimates of carbon emissions from thawing permafrost depend in large part on the ability of models to simulate present permafrost area extent (Brown et al., 1997). For example, the simulated permafrost in some models is significantly more sensitive to thaw, with corresponding larger esti-

TCD
9, 3137–3163, 2015

mates of carbon emissions (Koven et al., 2013). Narrowing the uncertainty in estimated carbon emissions requires improvements in how Land Surface Models (LSMs) represent permafrost thermal and carbon dynamics.

LSMs used to estimate emissions from thawing permafrost typically assume that the frozen carbon is located in the upper permafrost above 3 m depth and below the maximum active layer thickness (ALT) (Koven et al., 2011; Schaefer et al., 2011; MacDougall et al., 2012; Burke et al., 2013). Lacking spatially explicit maps of frozen carbon, these studies typically assumed a spatially uniform permafrost carbon density. The simulated ALT determines the volume of permafrost in the top 3 m of soil, and thus the initial amount of frozen carbon. Consequently, any biases in the simulated ALT strongly influence the initial amount of frozen carbon, even if different models assume the same permafrost carbon density. Also, positive biases in simulated ALT result in warmer soil temperatures, making the simulated permafrost more vulnerable to thaw and resulting in higher emissions estimates (Koven et al., 2013).

The surface organic layer (SOL) is the surface soil layer of nearly pure organic matter that exerts a huge influence on the thermodynamics of the active layer. The organic layer thickness (OLT) usually varies between 5–30 cm, depending on a balance between the litter accumulation rate relative to the organic matter decomposition rate (Yi et al., 2009; Johnstone et al., 2010). Recent model intercomparision study shows that LSMs need more realistic surface processes such as upper organic layer and better representations of subsoil thermal dynamics (Ekici et al., 2014a). The low thermal conductivity of the SOL makes it an effective insulator decreasing the heat exchange between permafrost and the atmosphere (Rinke et al., 2008). The effect of the SOL has been well presented in several modeling studies. For example, Lawrence and Slater (2008) showed that soil organic matter affects the permafrost thermal state in the Community Land Model (CLM), and Jafarov et al. (2012) discussed the effect of the SOL in the regional modeling study for Alaska, US. Recently, Chadburn et al. (2015a, b) incorporated the SOL in the Joint UK Land Environment Simulator (JULES) model to illustrate its influence on ALT and ground temperatures both at a site specific study

TCD
9, 3137–3163, 2015

in Siberia, Russia, and globally. In essence, the soil temperatures and ALT decrease as the OLT increases. Consequently, how (or if) LSMs represent the SOL in the simulated soil thermodynamics will simultaneously determine the initial amount of frozen permafrost carbon and the vulnerability of the simulated permafrost to thaw.

Here we describe a fully dynamic SOL to demonstrate the importance of coupling soil biogeochemistry and thermodynamics to improve the simulated permafrost temperature and ALT. We improved the Simple Biosphere/Carnegie–Ames–Stanford Approach (SiBCASA) model (Schaefer et al., 2011) by adding a dynamic SOL and limiting plant growth in frozen soils and demonstrate that these changes improve permafrost thermal and carbon dynamics in comparison. Then we use the modified model to evaluate current permafrost carbon stock (Hugeluis et al., 2014) under the steady state climate in the early 20th century.

2 Methods

We used the SiBCASA model (Schaefer et al., 2008) to evaluate current soil carbon stocks in permafrost affected soils. SiBCASA has fully integrated water, energy, and carbon cycles and computes surface energy and carbon fluxes at 10 min time steps. SiBCASA predicts the moisture content, temperature, and carbon content of the canopy, canopy air space, and soil (Sellers et al., 1996a; Vidale and Stockli, 2005). To calculate plant photosynthesis, the model uses a modified Ball–Berry stomatal conductance model (Ball, 1998; Collatz et al., 1991) coupled to a C3 enzyme kinetic model (Farquhar et al., 1980) and a C4 photosynthesis model (Collatz et al., 1992). It predicts soil organic matter, surface litter, and live biomass (leaves, roots, and wood) in a system of 13 prognostic carbon pools as a function of soil depth (Schaefer et al., 2008). The model biogeochemistry does not account for disturbances, such as fire, and does not include a nitrogen cycle. SiBCASA separately calculates respiration losses due to microbial decay (heterotrophic respiration) and plant growth (autotrophic respiration).

TCD
9, 3137–3163, 2015

SiBCASA uses a fully coupled soil temperature and hydrology model with explicit treatment of frozen soil water originally from the Community Climate System Model, Version 2.0 (Bonan, 1996; Oleson et al., 2004). To improve simulated soil temperatures and permafrost dynamics, Schaefer et al. (2009) increased the total soil depth to 15 m and added the effects of soil organic matter on soil physical properties. Simulated snow density and depth, and thus thermal conductivity, significantly influence simulated permafrost dynamics, so Schaefer et al. (2009) added the effects of depth hoar and wind compaction on simulated snow density and depth.

We spun SiBCASA up to steady-state initial conditions using an input weather dataset from the Climatic Research Unit National Center for Environmental Predictions (CRUNCEP) (Wei et al., 2014) for the entire permafrost domain in the Northern Hemisphere (Brown et al., 1997). CRUNCEP is modeled weather data at $0.5^{\circ} \times 0.5^{\circ}$ latitude and longitude resolution optimally consistent with a broad array of observations. The CRUNCEP dataset used in this study spans 110 years, from 1901 to 2010. We selected the first 30 years from the CRUNCEP dataset (1901 to 1931) and randomly distributed them over 900 years. To run our simulations we used JANUS High Performance Computing (HPC) Center at University of Colorado at Boulder. The 900 yr time span was chosen in order to make optimal use of the computational time, which allowed us to finish one spinup simulation within 24 h, the maximum allocated time at the JANUS HPC node to run the model without interruptions.

2.1 Frozen carbon initialization

The Permafrost Research Coordination Network (Hugeluis et al., 2013) published a revised Northern Circumpolar Soil Carbon Dataset version 2 (NCSCDv2). The NCSCDv2 includes soil carbon density maps in permafrost-affected soils available at several spatial resolutions ranging from 0.012 to 1°. The dataset comprise spatially extrapolated soil carbon data from more than 1700 soil core samples. This dataset has three main layers each 1 m in depth, distributed between ground surface and 3 m depth.

TCD
9, 3137–3163, 2015

We placed the frozen carbon within the top three meters of simulated permafrost, ignoring deltaic and loess deposits that are known to extend well beyond 3 m of depth (Hugelius et al., 2014). The bottom of the permafrost carbon layer is fixed at 3 m, while the top varies spatially with changes in ALT during the spinup run. Defining the permafrost table as the maximum thaw depth, we essentially assume that the soil above the permafrost table has thawed frequently enough over thousands of years to decay away all the old carbon.

We initialized frozen carbon between the permafrost table and 3 m depth using two scenarios: (1) spatially uniform distribution of the frozen carbon throughout the permafrost domain (Schaefer et al., 2011), and (2) observed distribution of the frozen carbon according to the NCSCDv2. The total initial frozen carbon in each soil layer between the permafrost table and 3 m is

$$C^i_{\mathrm{fr}} = \rho_{\mathrm{c}} \Delta z_i, \tag{1}$$

where C^i_{fr} is the total permafrost carbon within the ith soil layer, ρ_{c} is the permafrost carbon density, and Δz_i is the thickness of the ith soil layer in the model. For the uniform permafrost carbon distribution, $\rho_{\mathrm{c}} = 21\,\mathrm{kg\,C\,m^{-3}}$ assumed to be spatially and vertically uniform (Schaefer et al., 2011). For the observed distribution from the NCSCDv2, ρ_{c} varies both with location and depth (Hugeluis et al., 2013).

$$\begin{aligned} C^i_{\mathrm{slow}} &= 0.8 C^i_{\mathrm{fr}} \\ C^i_{\mathrm{met}} &= 0.2 f_{\mathrm{root2met}} C^i_{\mathrm{fr}} \\ C^i_{\mathrm{str}} &= 0.2 f_{\mathrm{root2strt}} C^i_{\mathrm{fr}}, \end{aligned} \tag{2}$$

where f_{root2met} and $f_{\mathrm{root2strt}}$ are the simulated fractions of root pool losses to the soil metabolic and structural pools respectively (Schaefer et al., 2008). Note that Schaefer et al. (2011) has a 5 % loss to the metabolic pool and a 15 % loss to the structural pool based on observed values in Dutta et al. (2006). The simulated fractions are actually 5.6 % to the metabolic pool and 14.4 % to the structural pool. We found it encouraging

TCD
9, 3137–3163, 2015

that the numbers calculated with the SiBCASA metabolic fractions resulted in numbers that are close to the observed values in Dutta et al. (2006).

2.2 Dynamic SOL

We modified SiBCASA to include a dynamic SOL by incorporating the vertical redistribution of organic material associated with soil accumulation. SiBCASA already accounted for the effects of organic matter on soil properties like porosity, hydraulic conductivity, and thermal conductivity. To allow vertical movement and build up a SOL, we placed a maximum limit on the amount of organic material that each soil layer can hold. When the simulated carbon content exceeds this threshold, the excess carbon is transferred to the layer below. This is a highly simplified version of the Koven et al. (2011) carbon diffusion model, which accounts for all sedimentation and cryoturbation processes, while we wanted to limit our model only to the buildup of a SOL. We calculate the maximum allowed carbon content per soil layer, C_{max}, as

$$C_{max} = \rho_{max} f_C \Delta z \frac{1000}{MW_C}, \quad (3)$$

where ρ_{max} is the maximum density of pure organic matter or peat, f_c is the fraction of organic matter that is carbon, Δz is the soil layer thickness (m), MW_C is the molecular weight of carbon ($12\,g\,mol^{-1}$), and the factor of 10^3 converts from grams to kilograms. The MW_C term converts the expression into mol C m^{-2}, the SiBCASA internal units for carbon. The simulated organic soil fraction per soil layer, f_{org}, is defined as

$$f_{org} = \frac{C}{f_c C_{max}}, \quad (4)$$

where C is the carbon content per soil layer ($mol\,m^{-2}$). Based on observations of bulk densities of peat, we assume C_{max}, is $140\,kg\,m^{-3}$ (Price et al., 2005). C_{max} is bulk density, so to convert to carbon we assume f_c is 0.5, which assumes that half of the

TCD
9, 3137–3163, 2015

organic matter by mass is carbon. The original formulation allowed f_{org} to exceed 1.0 such that the excess organic material was essentially "compressed" into the top soil layer, resulting in a 2 cm simulated SOL. We place an upper limit of 0.95 on f_{org} and transfer the excess carbon to the layer below. The OLT is defined as the bottom of the lowest soil layer where f_{org} is 0.95. OLT_{max} is the theoretical maximum thickness of the SOL, assuming all organic matter for the entire soil column is concentrated at the surface

$$OLT_{max} = \frac{C_{tot}}{\rho_{max} f_C} \frac{MW_C}{1000}. \quad (5)$$

2.3 Root growth and soil thermal factor

In the original formulation (without dynamic SOL), plant photosynthesis, leaf growth, and fine root growth were controlled primarily by canopy air space temperature: when the canopy air temperature exceeded 0 °C, leaves and roots started to grow. SiBCASA assumes fine root growth decreases exponentially with depth based on observed vertical root distributions (Schaefer et al., 2008) with 90 % of fine root growth occurring in the top 1 m of soil. Since soil thaw starts after the canopy warms and the snow melts, this results in unrealistic simulated fine root growth in frozen soil. Photosynthesis is limited by water availability as well as canopy temperature and starts later in spring after the surface soil layers thaw out. The result is an unrealistic delay between the start of photosynthesis in spring and the timing of simulated leafout and root growth.

We synchronized leafout, root growth, and photosynthesis by restricting root growth to occur only in thawed soil layers. In SiBCASA, leaf growth is linked to fine root growth (Schaefer et al., 2008), so this also delays spring leafout until the soil begins to thaw. We first calculated the fraction of thawed roots:

$$R_{th} = \sum_{k=1}^{nroot} R_f(1 - F_{ice}), \quad (6)$$

TCD
9, 3137–3163, 2015

where R_{th} is the fraction of total roots that are thawed, nroot is the deepest soil layer with roots, R_f is the reference root fraction per soil layer based on observed root distributions (Jackson et al., 1996), and F_{ice} is the ice fraction per soil layer. This assumes that water in each layer is evenly distributed such that F_{ice} equals the frozen fraction (when $F_{ice} = 0$, the soil layer is completely thawed).

Restricting root growth within the thawed portion of the active layer results from the fact that roots cannot penetrate frozen soil. Root growth still decreases exponentially with depth, but we used an effective rooting depth equal to the thaw depth or the theoretical maximum rooting depth from the exponential soil distributions (whichever is less). We calculated an effective root fraction R_{eff}, to control the vertical distribution of new growth carbon within the soil column:

$$R_{eff} = R_f (1 - F_{ice}) / R_{th}. \quad (7)$$

Dividing by R_{th} ensures that R_{eff} sums to one within the soil column, which essentially ensures that all new root growth is distributed only within the thawed portion of the soil column. Here, we replaced R_f with R_{eff} in the vertical distribution of coarse woody roots in the wood pool and the fine roots in the root pool and associated calculations of autotrophic respiration.

To synchronize growth primary productivity (GPP) with leafout, we treated the reference vertical root distribution, R_f, as the potential root growth defining the maximum potential GPP. Since the sum of R_f is always one, when $R_{th} < 1$, GPP must be less than its full potential. We defined a GPP scaling factor, $S_{soilfrz}$, as

$$S_{soilfrz} = \begin{cases} R_{th}, & R_{th} \geq 0.01 \\ 0, & R_{th} < 0.01 \end{cases}. \quad (8)$$

This assumes that at least 1 % of the roots must be thawed for GPP to occur, corresponding to about ~ 1 cm of thawed soil. $S_{soilfrz}$ is applied along with the soil moisture and canopy temperature scaling factors to constrain photosynthesis while soil is frozen

TCD
9, 3137–3163, 2015

(Schaefer et al., 2008). To constrain wood growth, we applied $S_{soilfrz}$ to the temperature scaling factors to the decay rate constant that controls wood growth

$$k_{eff} = S_{nsc} S_T S_M S_{frost} S_{soilfrz} k_{wood}, \quad (9)$$

where k_{eff} is the effective growth rate, S_{nsc} is the non-structural carbohydrate scaling factor, S_T is the canopy temperature scaling factor, S_{frost} is the frost inhibition function, and k_{wood} is the reference wood growth rate. S_T, S_{frost}, and $S_{soilfrz}$ are the same scaling factors that control GPP under the assumption that the factors that control photosynthesis also control wood growth (Schaefer et al., 2008). This is also consistent with what we normally see in discontinuous permafrost zones: trees cannot grow in shallow permafrost. Indeed, one can often detect the presence of permafrost in the discontinuous zone simply by noting the lack of trees.

To constrain leaf growth, we added $S_{soilfrz}$ to the frozen leaf scaling factor

$$S_{leaffrz} = S_{soilfrz}/(1 + \exp(1.3(273 - T_{can}))), \quad (10)$$

where $S_{leaffrz}$ is the frozen leaf scaling factor and T_{can} is canopy temperature.

3 Results

The dynamic SOL decreased the simulated ALT on average 50 % across the domain and allowed the model to simulate permafrost in discontinuous zones where it could not before (Fig. 1). The area of near surface permafrost simulated with the current version of the model equals to 13.5 mil km^2 which is almost 38 % greater than without the dynamic SOL (Schaefer et al., 2011). This area is closer to the observation from the International Permafrost Association which is about 16.2 mil km^2 (Brown et al.,1997). Simulated ALT less than 2 m covers about 92 % of the area in the new simulations (Fig. 1b) in comparison to 66 % of the area in the Schaefer et al. (2011) simulations (Fig. 1a). The previous version of SiBCASA could not simulate permafrost in many

TCD
9, 3137–3163, 2015

parts of the discontinuous zone with relatively warm climate. Adding the dynamic SOL essentially decreased the thermal conductivity of the surface soil to allow SiBCASA to simulate permafrost where the mean annual air temperatures (MAAT) are close to 0 °C.

To illustrate the improvement of the simulated ALT with respect to the observed data, we compared simulated ALT with measured values from Circumpolar Active Layer Monitoring (CALM) stations. The CALM network is a part of the Global Terrestrial Network for Permafrost (GTN-P) (Burgess et al., 2000). The monitoring network measures ALT either using a mechanical probe or a vertical array of temperature sensors (Brown et al., 2000; Shiklomanov et al., 2010). After matching up the CALM coordinates with the coordinates of previously simulated ALT (Schaefer et al., 2011), we excluded sites with no measurements or ALT greater than 3 m depth, ending up with 76 CALM stations. Figure 2 shows simulated vs. observed ALT for the 76 CALM sites. The current simulations have a higher resolution than Schaefer et al. (2011) simulations, so the effect is not as pronounced. The Pearson's correlation coefficient, R, is negative and not significant for the Schaefer et al. (2011) simulations (Fig. 2a), but is positive and statistically significant for the current simulations assuming $p < 0.05$ (Fig. 2b). The dynamic SOL greatly improves the simulated ALT, but SiBCASA still tends to overestimate ALT.

Figure 3 illustrates the effect of the frozen soil restrictions on phenology and GPP at a single point in central Siberia. Before applying a frozen soil restriction, SiBCASA maintained fine roots even in winter, resulting in root growth all year with a strong peak in spring corresponding to simulated leafout (Fig. 3a). Simulated GPP was restricted by liquid water availability and was closely tied to thawing of the active layer, resulting in a lag as high as 60 days between leafout and start of GPP in spring. Restricting growth and GPP to when the soil is thawed essentially synchronizes all phenological events to occur at the same time (Fig. 3b).

The dynamic SOL introduced a strong coupling between ALT and GPP via plant root growth in the areas with deciduous and mixed forest biomes (southern margins of the permafrost domain Fig. 1a). The relatively high GPP of the forest and associated litterfall resulted in a thick SOL. The high porosity of organic matter resulted in higher

TCD
9, 3137–3163, 2015

soil water content, which decreased the ALT and allowed root growth to occur directly into the permafrost. This coupling was entirely a numerical feedback that does not reflect reality, but took several thousand years of spinup to become obvious. The frozen soil restrictions on GPP and growth eliminated this GPP-ALT feedback. After another 4500 years of spinup, the only sign of this feedback that remained was a shallow ALT in South-Central Siberia.

Restricting growth and GPP to when the soil is thawed delayed the onset of plant photosynthesis in spring in permafrost-affected regions. Introduction of the thawed root fraction in the model reduced GPP primarily in early spring. To illustrate the difference between unconstrained and restricted root growth (Fig. 3), we ran the model for ten years for both cases. The difference between unconstrained and restricted root growth cases (Fig. 4) indicates an overall ~ 9 % reduction in GPP for the entire permafrost domain, nearly all of which occurred in spring.

The decrease in ALT resulting from a dynamic SOL increases the volume of permafrost in the top 3 m of soil, greatly increasing the initial amount of frozen permafrost carbon in the simulations. Schaefer et al. (2011) without the dynamic SOL assumed a uniform permafrost carbon density of 21 kg C m^{-3}, resulting in a total of 313 Gt of permafrost carbon at the start of their transient run (Fig. 5a). To compare the overall permafrost carbon storage, we equilibrated the current version of the model assuming similar uniform distribution (Fig. 5b). Assuming the same uniform carbon density, the current version with the dynamic SOL results in a total of ~ 680 Gt C compared to 313 Gt C in Schaefer et al. (2011). The dynamic SOL effectively doubled the volume of permafrost in the top three meters of soil and the amount of simulated frozen carbon.

Initializing SiBCASA with the observed spatial distribution of permafrost carbon from the NCSCDv2 resulted in ~ 560 Gt C of carbon stored in permafrost after spinup (Fig. 6a). SiBCASA underestimated the SOC in the Eastern Canada and Western Siberia, and overestimated SOC in Central Siberia. Failure to simulate soil carbon in South-East Canada and South-West Siberia (Fig. 6b) could be attributed to deep active layer thickness, where overestimation of the SOC in Central Siberia occurs due to

TCD
9, 3137–3163, 2015

high SOC at the initial time step. The overall amount of soil frozen carbon is less than that calculated assuming uniform frozen carbon distribution. It is important to note that the ALT and the permafrost thickness in both cases (Figs. 5b and 6a) are identical. The smaller permafrost carbon stock simulated for the non-uniform case is mainly due to the fact that we did not initialize frozen carbon in regions where according to the NCSCDv2 it is not present, such as the Brooks Range in Alaska.

4 Discussion

The dynamic SOL insulates ALT from air temperature, allowing SiBCASA to simulate permafrost in many discontinuous permafrost regions where it could not before. This result complements similar findings by Lawrence and Slater (2008), Yi et al. (2009), Ekici et al., (2014b), and Chadburn et al. (2015a, b), when changes in thermal properties associated with the presence of soil organic matter cooled the ground. In Southeastern Canada and Southwestern Siberia, SiBCASA simulates ALT up to 3 m, and therefore almost no frozen carbon. For example, observed mean annual ground temperatures within Southeast Canada region ranges from below to above 0 °C (Smith, and Burgess, 2000), which suggests that the actual permafrost distribution and associated ALT in these regions would be highly heterogeneous. Models like SiBCASA cannot capture such sub-grid heterogeneity, resulting in a deeper, uniform ALT across the grid cell.

The most influential factor on the ALT is the near surface air temperature (NSAT). To show this influence, we averaged NSAT in early fall, for two months September and October over 10 years (Fig. 7a). The areas with deep ALT (Fig. 1b) fall into the regions where NSATs are greater than one degree centigrade and greater than 5 °C in the South-East Canada. The downward longwave radiation is another important source of energy contributing to increase in the surface temperatures. Averaged over 10 years, downward longwave radiation is higher along the south boundaries of the domain, in particular South-East Canada and South-West Siberia (Fig. 7b). Another significant

TCD
9, 3137–3163, 2015

factor contributing to the warm ground temperatures is snow depth. Figure 7c shows maximum simulated snow depth calculated over the last 10 years of the steady state run. It is clear that in West Siberia, snow provides significant insulation during winter period and contributes to warmer ground temperatures. However, maximum snow depth in South-East Canada is almost half that of West Siberia, which suggest that snow in South-East Canada, most likely, is not a major contributor to warm ground temperatures. Figure 7d shows an averaged soil wetness map, which indicates high wetness factor in both regions where model simulates deep ALT. This suggests that SOL does not provide enough protection for permafrost in regions with wet soils and mild air temperatures. This complements similar funding by Lawrence and Slater (2008).

Before implementing the dynamic SOL, the maximum rooting depth only occasionally fell below the permafrost table. However, after implementing the dynamic SOL, the simulated ALT decreased and new root growth was placed directly into the permafrost with no chance to decay. This phenomenon occurred primarily in the mixed deciduous evergreen forest in South-Central Siberia and resulted in a long-term carbon sink into the permafrost carbon pool. It resulted from the fact that the maximum rooting depth determined by the fixed, exponential root distribution incorrectly extended into the permafrost.

In permafrost-affected soils, seasonal root growth is largely regulated by the soil thermal conditions (Tryon and Chapin, 1983; Van Cleve et al., 1983). Therefore in the LSMs it is important to restrict root growth to thawed soil layers only. Moreover, previous studies showed that the date of snowmelt usually determines the start date of the growing season and the start of active layer thawing (Grøndahl et al., 2007; Wipf and Rixen, 2010). Restricting GPP and all growth using the scaling factors described above synchronizes the simulated start of the growing season.

The ability of the ecosystem and climate models to reproduce current frozen soil carbon distribution is important and could reduce uncertainty associated with modeling of the permafrost carbon feedback. Simulated permafrost vulnerability is tightly coupled with the accurate modeling of the present permafrost distribution. SiBCASA can barely

TCD
9, 3137–3163, 2015

simulate permafrost in regions with wet soils and mild climate, such as Southeastern Canada and Southwestern Siberia (Fig. 1a). We surmise that the CRUNCEP data may not place the 0 °C MAAT isotherm at the correct latitudes to match with the southern edge of discontinuous permafrost. The carbon rich soils in these regions may have already begun to thaw, which means that these regions may be currently respiring to the atmosphere and will continue to respire during this century.

5 Conclusions

Including a dynamic SOL is crucial to properly simulate permafrost dynamics and associated biogeochemistry. Strong coupling between ALT and plant root growth improved simulation of the ALT and soil carbon. Constraining root growth to thawed soil layers reduced the overall GPP by 9 % and synchronized the simulated phenology.

The NSDSCv2 indicates high carbon density in Southeastern Canada and Southwestern Siberia. Our modeling results show low soil carbon distribution in those areas, which is a result of deep ALT. The initialized soil carbon respired during spinup due to abundance of permafrost within the top 3 m. This could suggest that soil carbon in these locations is not steady state and currently actively respiring to the atmosphere.

Acknowledgements. This research was funded by NOAA grant NA09OAR4310063 and NASA grant NNX10AR63G. This work utilized the Janus supercomputer, which is supported by the National Science Foundation (award number CNS-0821794) and the University of Colorado Boulder. We thank K. Gregory at NSIDC for reviewing the manuscript.

TCD
9, 3137–3163, 2015

References

Ball, J. T.: An analysis of stomatal conductance, PhD thesis, Stanford Univ., Stanford, CA., 1988.

Bonan, G. B.: A Land Surface Model (LSM Version 1.0) for ecological, hydrological, and atmospheric studies: technical description and users guide, NCAR Tech. Note NCAR/TN-417+STR, Natl. Cent. for Atmos. Res., Boulder, CO, 1996.

Brown, J., Ferrians Jr., O. J., Heginbottom, J. A., and Melnikov, E. S. (Eds.): Circum-Arctic Map of Permafrost and Ground-Ice Conditions, US Geological Survey in Cooperation with the Circum-Pacific Council for Energy and Mineral Resources, Circum-Pacific Map Series CP-45, scale 1 : 10,000,000, 1 sheet, US Geological Survey, Boulder, Colorado, USA, 1997.

Brown, J., Hinkel, K., and Nelson, F.: The 1 Circumpolar Active Layer Monitoring (CALM) program: research designs and initial results, Polar Geogr., 24, 165–258, doi:10.1080/10889370009377698, 2000.

Bonan, G. B.: A Land Surface Model (LSM Version 1.0) for ecological, hydrological, and atmospheric studies: technical description and users guide. NCAR Technical Note NCAR/TN-417+STR, Boulder, CO, 1996.

Burgess, M. M., Smith, S. L., Brown, J., Romanovsky, V., and Hinkel, K.: The Global Terrestrial Network for Permafrost (GTNet-P): Permafrost Monitoring Contributing to Global Climate Observations, available online: http://ftp2.cits.rncan.gc.ca/pub/geott/ess_pubs/211/211621/cr_2000_e14.pdf, last access: 9 June 2015.

Burke, E. J., Hartley, I. P., and Jones, C. D.: Uncertainties in the global temperature change caused by carbon release from permafrost thawing, The Cryosphere, 6, 1063–1076, doi:10.5194/tc-6-1063-2012, 2012.

Callaghan, T. V., Johansson, M., Anisimov, O., Christiansen, H. H., Instanes, A., Romanovsky, V., and Smith, S.: Chapter 5: Changing permafrost and its impacts. in: Snow, Water, Ice and Permafrost in the Arctic (SWIPA) 2011. Arctic Monitoring and Assessment Programme (AMAP), Oslo, 62 pp., 2011.

Chadburn, S., Burke, E., Essery, R., Boike, J., Langer, M., Heikenfeld, M., Cox, P., and Friedlingstein, P.: An improved representation of physical permafrost dynamics in the JULES land-surface model, Geosci. Model Dev., 8, 1493–1508, doi:10.5194/gmd-8-1493-2015, 2015a.

Chadburn, S. E., Burke, E. J., Essery, R. L. H., Boike, J., Langer, M., Heikenfeld, M., Cox, P. M., and Friedlingstein, P.: Impact of model developments on present and future simulations

TCD
9, 3137–3163, 2015

of permafrost in a global land-surface model, The Cryosphere Discuss., 9, 1965–2012, doi:10.5194/tcd-9-1965-2015, 2015b.
Collatz, G. J., Ball, J. T., Grivet, C., and Berry, J. A.: Physiological and environmental regulation of stomatal conductance, photosynthesis, and transpiration: a model that includes a laminar boundary layer, Agr. Forest Meteorol., 54, 107–136, doi:10.1016/0168-1923(91)90002-8, 1991.
Collatz, G. J., Ribascarbo, M., and Berry, J. A.: Coupled photosynthesis-stomatal conductance model for leaves of C4 plants, Aust. J. Plant Physiol., 19, 519–538, 1992.
Dutta, K., Schuur, E. A. G., Neff, J. C., and Zimov, S. A.: Potential carbon release from permafrost soils of Northeastern Siberia, Global Change Biol., 12, 2336–2351, 2006.
Ekici, A., Chadburn, S., Chaudhary, N., Hajdu, L. H., Marmy, A., Peng, S., Boike, J., Burke, E., Friend, A. D., Hauck, C., Krinner, G., Langer, M., Miller, P. A., and Beer, C.: Site-level model intercomparison of high latitude and high altitude soil thermal dynamics in tundra and barren landscapes, The Cryosphere Discuss., 8, 4959–5013, doi:10.5194/tcd-8-4959-2014, 2014a.
Ekici, A., Beer, C., Hagemann, S., Boike, J., Langer, M., and Hauck, C.: Simulating high-latitude permafrost regions by the JSBACH terrestrial ecosystem model, Geosci. Model Dev., 7, 631–647, doi:10.5194/gmd-7-631-2014, 2014b.
Farquhar, G. D., von Caemmerer, S., and Berry, J. A.: A biochemical model of photosynthetic CO_2 assimilation in leaves of C3 species, Planta, 149, 78–90, doi:10.1007/BF00386231, 1980.
Grøndahl, L., Friborg, T., and Soegaard, H.: Temperature and snow-melt controls on interannual variability in carbon exchange in the high Arctic, Theor. Appl. Climatol., 88, 111–125, 2007.
Hugelius, G., Tarnocai, C., Broll, G., Canadell, J. G., Kuhry, P., and Swanson, D. K.: The Northern Circumpolar Soil Carbon Database: spatially distributed datasets of soil coverage and soil carbon storage in the northern permafrost regions, Earth Syst. Sci. Data, 5, 3–13, doi:10.5194/essd-5-3-2013, 2013.
Hugelius, G., Strauss, J., Zubrzycki, S., Harden, J. W., Schuur, E. A. G., Ping, C.-L., Schirrmeister, L., Grosse, G., Michaelson, G. J., Koven, C. D., O'Donnell, J. A., Elberling, B., Mishra, U., Camill, P., Yu, Z., Palmtag, J., and Kuhry, P.: Estimated stocks of circumpolar permafrost carbon with quantified uncertainty ranges and identified data gaps, Biogeosciences, 11, 6573–6593, doi:10.5194/bg-11-6573-2014, 2014.

TCD
9, 3137–3163, 2015

Jafarov, E. E., Marchenko, S. S., and Romanovsky, V. E.: Numerical modeling of permafrost dynamics in Alaska using a high spatial resolution dataset, The Cryosphere, 6, 613–624, doi:10.5194/tc-6-613-2012, 2012.

Jackson, R. B., Canadell, J., Ehleringer, J. R., Mooney, H. A., Sala, O. E., and Schulze, E. D.: A global analysis of root distributions for terrestrial biomes, Oecologia, 108, 389–411, doi:10.1007/BF00333714, 1996.

Johnstone, J. F., Chapin III, F. S., Hollingsworth, T. N., Mack, M. C., Romanovsky, V., and Turetsky, M.: Fire, climate change, and forest resilience in interior Alaska, Can. J. Forest Res., 40, 1302–1312, 2010.

Koven, C. D., Friedlingstein, P., Ciais, P., Khvorostyanov, D., Krinner, G., and Tarnocai, C.: On the formation of high-latitude soil carbon stocks: effects of cryoturbation and insulation by organic matter in a land surface model, Geophys. Res. Lett., 36, L21501, doi:10.1029/2009GL040150, 2009.

Koven, C. D., Ringeval, B., Friedlingstein, P., Ciais, P., Cadule, P., Khvorostyanov, D., Krinner, G., and Tarnocai, C.: Permafrost carbon-climate feedbacks accelerate global warming, P. Natl. Acad. Sci. USA, 108, 14769–14774, doi:/10.1073/pnas.1103910108, 2011.

Koven, C. D., Riley, W. J., and Stern, A.: Analysis of permafrost thermal dynamics and response to climate change in the CMIP5 earth system models, J. Climate, 26, 1877–1900, doi:10.1175/JCLI-D-12-00228.1, 2013.

Lawrence, D. M. and Slater, A. G.: Incorporating organic soil into a global climate model, Clim. Dynam., 30, 145–160, doi:10.1007/s00382-007-0278-1, 2008.

MacDougall, A. H., Avis, C. A., and Weaver, A. J.: Significant contribution to climate warming from the permafrost carbon feedback, Nat. Geosci., 5, 719–721, doi:10.1038/NGEO1573, 2012.

Oberman, N. G.: Contemporary Permafrost Degradation of Northern European Russia, in: Proceedings Ninth International Conference on Permafrost, Vol. 2, Fairbanks, Alaska, USA, 1305–1310, 2008.

Oleson, K. W., Lawrence, D. M., Bonan, G. B., Flanner, M. G., Kluzek, E., Lawrence, P. J., Levis, S., Swenson, S. C., Thornton Aiguo Dai, P. E., Decker, M., Dickinson, R., Feddema, J., Heald, C. L., Hoffman, F., Lamarque, J.-F., Mahowald, N., Niu, G.-Y., Qian, T., Randerson, J., Running, S., Sakaguchi, K., Slater, A., Stöckli, R., Wang, A., Yang, Z. L., Zeng, X., and Zeng, X.: Technical description of the Community Land Model (CLM), NCAR Tech. Note TN-461+STR, National Center for Atmospheric Research, Boulder, Colorado, 174 pp., 2004.

TCD
9, 3137–3163, 2015

Price, J. S., Cagampan, J., and Kellner, E.: Assessment of peat compressibility: is there an easy way?, Hydrol. Process., 19, 3469–3475, 2005.

Sellers, P. J., Randall, D. A., Collatz, G. J., Berry, J. A., Field, C. B., Dazlich, D. A., Zhang, C., Collelo, G. D., and Bounoua, L.: A revised land surface parameterization of GCMs, Part I: model formulation, J. Climate, 9, 676–705, 1996.

Schaefer, K., Collatz, G. J., Tans, P., Denning, A. S., Baker, I., Berry, J., Prihodko, L., Suits, N., and Philpott, A.: The combined Simple Biosphere/Carnegie–Ames–Stanford Approach (SiBCASA) Model, J. Geophys. Res., 113, G03034, doi:10.1029/2007JG000603, 2008.

Schaefer, K., Zhang, T., Slater, A. G., Lu, L., Etringer, A., and Baker, I.: Improving simulated soil temperatures and soil freeze/thaw at high-latitude regions in the Simple Biosphere/Carnegie–Ames–Stanford Approach model, J. Geophys. Res., 114, F02021, doi:10.1029/2008JF001125, 2009.

Schaefer, K., T. Zhang, L. Bruhwiler, and A. P. Barrett.: Amount and timing of permafrost carbon release in response to climate warming, Tellus B, 63, 165–180, doi:10.1111/j.1600-0889.2011.00527.x, 2011.

Schaefer, K., Lantuit, H., Romanovsky, V. E., Schuur, E. A. G., and Witt, R.: The impact of the permafrost carbon feedback on global climate, Environ. Res. Lett., 9, 085003, doi:10.1088/1748-9326/9/8/085003, 2014.

Shiklomanov, N. I., Streletskiy, D. A., Nelson, F. E., Hollister, R. D., Romanovsky, V. E., Tweedie, C. E., Bockheim, J. G., and Brown, J.: Decadal variations of active-layer thickness in moisture-controlled landscapes, Barrow, Alaska, J. Geophys. Res., 115, G00I04, doi:doi:10.1029/2009JG001248, 2010.

Schuur,E. A. G., McGuire, A. D., Schädel, C., Grosse, G., Harden, J. W., Hayes, D. J., Hugelius, G., Koven, C. D., Kuhry, P., Lawrence, D. M., Natali, S. M., Olefeldt, D., Romanovsky, V. E., Schaefer, K., Turetsky, M. R., Treat, C. C., and Vonk, J. E.: Climate change and the permafrost carbon feedback, Nature, 520, 171–179, doi:10.1038/nature14338, 2015.

Smith, S. and Burgess, M. M.: Ground Temperature Database for Northern Canada, Geological Survey of Canada, Open File Report No. 3954, Geological Survey of Canada, http://geoscan.nrcan.gc.ca/starweb/geoscan/servlet.starweb?path=geoscan/fulle.web&search1=R=211804 (last access: June 2015), 1–28, 2000.

TCD
9, 3137–3163, 2015

Tarnocai, C., Canadell, J. G., Schuur, E. A. G., Kuhry, P., Mazhitova, G., and Zimov, S.: Soil organic carbon pools in the northern circumpolar permafrost region, Global Biogeochem. Cy., 23, GB2023, doi:10.1029/2008GB003327, 2009.

Tryon, P. and Chapin III, F.: Temperature controls over root growth and root biomass in taiga forest trees, Can. J. Forest Res., 13, 827–33, 1983.

Van Cleve, K. L., Oliver, L., Schlentner, R., Viereck, L., and Dyrness, C. T.: Productivity and nutrient cycling in tiaga forest exosystems, Can. J. Forest Res., 13, 747–766, 1983.

Vidale, P. L. and Stockli, R.: Prognostic canopy air space solutions for land surface exchanges, Theor. Appl. Climatol., 80, 245–257, 2005.

Wei, Y., Liu, S., Huntzinger, D. N., Michalak, A. M., Viovy, N., Post, W. M., Schwalm, C. R., Schaefer, K., Jacobson, A. R., Lu, C., Tian, H., Ricciuto, D. M., Cook, R. B., Mao, J., and Shi, X.: The North American Carbon Program Multi-scale Synthesis and Terrestrial Model Intercomparison Project – Part 2: Environmental driver data, Geosci. Model Dev., 7, 2875–2893, doi:10.5194/gmd-7-2875-2014, 2014.

Wipf, S. and Rixen, C.: A review of snow manipulation experiments in Arctic and alpine tundra ecosystems, Polar Res., 29, 95–109, doi:10.1111/j.1751-8369.2010.00153.x, 2010.

Yi, S., Manies, K., Harden, J., and McGuire, A. D.: Characteristics of organic soil in black spruce forests: implications for the application of land surface and ecosystem models in cold regions, Geophys. Res. Lett., 36, L05501, doi:10.1029/2008GL037014, 2009.

TCD
9, 3137–3163, 2015

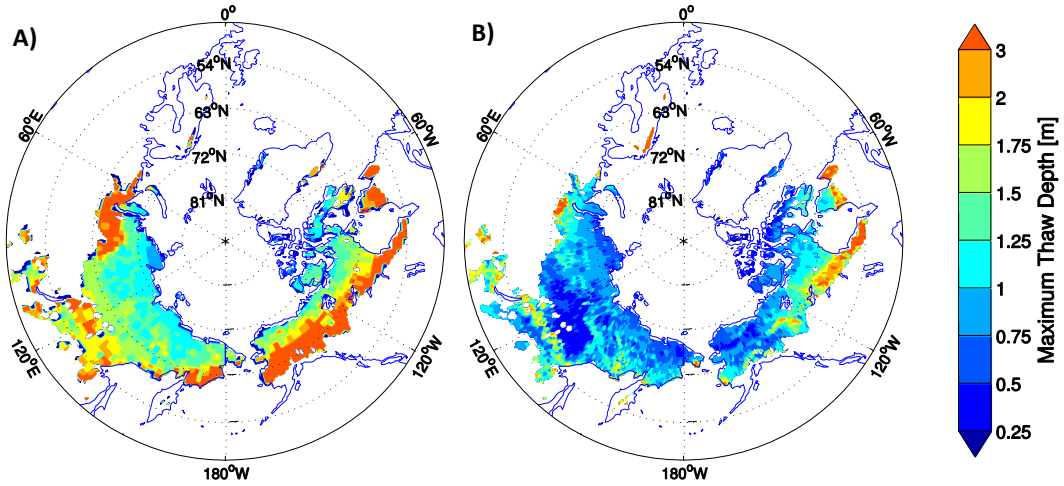

Figure 1. Maximum thaw depth averaged over last five years after spinup from **(a)** Schaefer et al. (2011) and **(b)** this study, in m.

TCD
9, 3137–3163, 2015

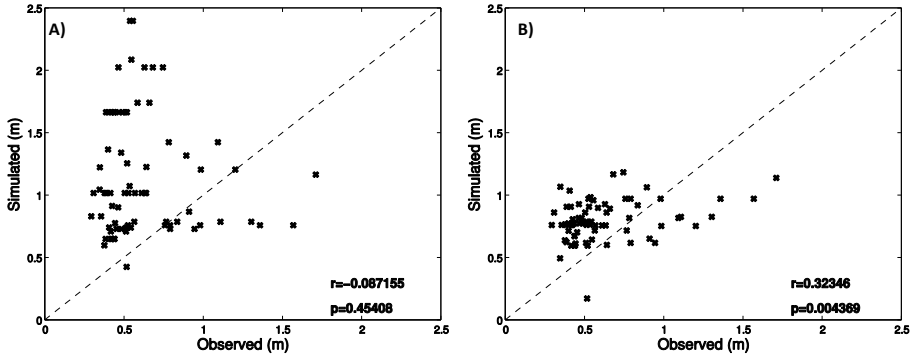

Figure 2. Comparison of the mean active layer thickness (ALT) from 76 Circumpolar Active Layer Monitoring stations with the averaged ALT from last five years after spinup from **(a)** Schaefer et al. (2011) and **(b)** this study. r is a Pearson's correlation coefficient and p is a significance value, $p < 0.05$ stands for the 95 % of confidence.

TCD
9, 3137–3163, 2015

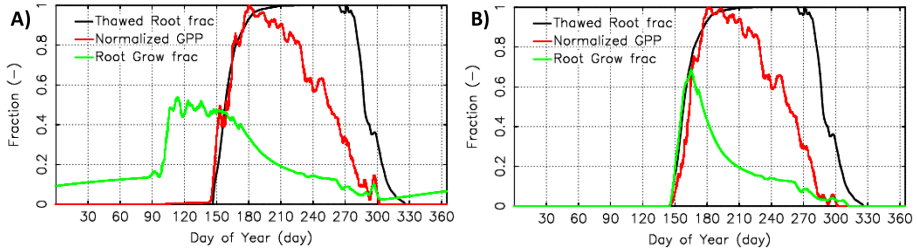

Figure 3. (a) and **(b)** root growth without and with the frozen soil constraint on growth.

TCD
9, 3137–3163, 2015

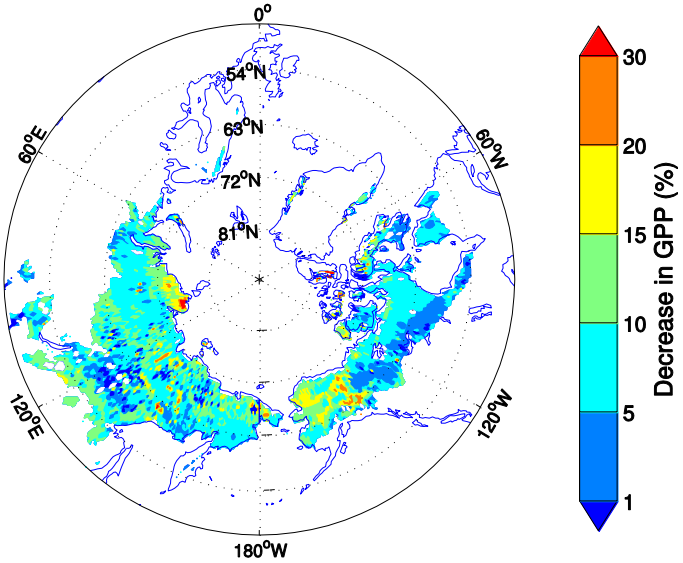

Figure 4. The difference between GPP without and with freezing constraint averaged over ten years.

TCD
9, 3137–3163, 2015

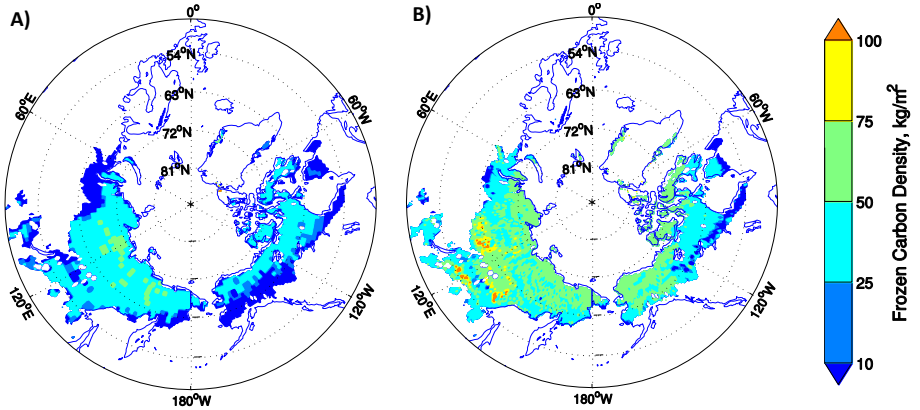

Figure 5. The frozen carbon maps obtained assuming uniform frozen carbon distribution at the initial time step, and averaged over five years at the end of the steady state run: **(a)** from Schaefer et al. (2011), and **(b)** from the current run, correspondingly.

TCD
9, 3137–3163, 2015

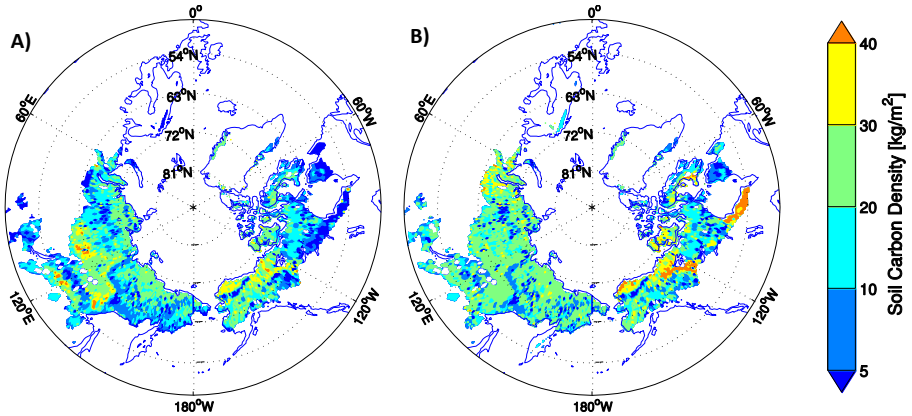

Figure 6. The soil carbon maps averaged over top 3 m: **(a)** from SiBCASA at the end of the steady state run, and **(b)** from the NCSCDv2, correspondingly.

TCD
9, 3137–3163, 2015

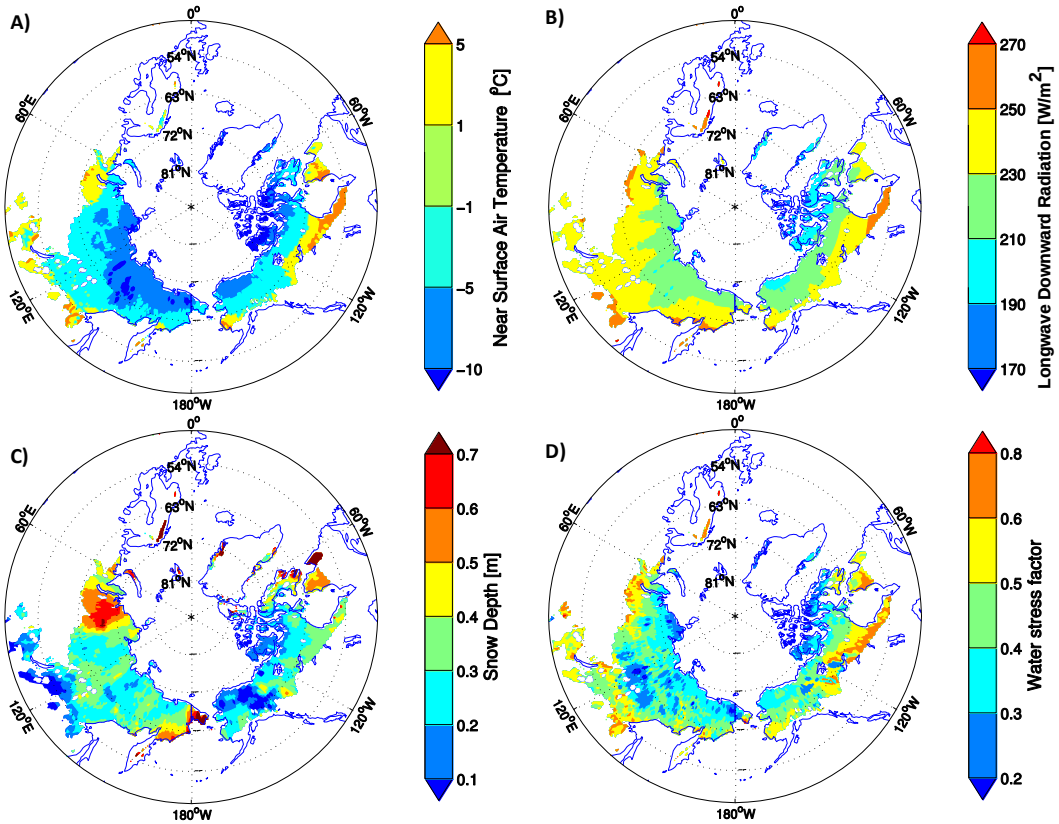

Figure 7. (a) The canopy air space temperature for averaged over September and November, and **(b)** the down-welling long-wave radiation, averaged yearly over 10 years. **(c)** The maximum snow depth over 10 years for the steady state run, and **(d)** the water stress factor (non-dimensionless fraction of 1), averaged yearly over 10 years.

TCD
9, 3137–3163, 2015